

Model Predictive Control of Vapor Compression Systems

Burns, D.J.; Danielson, C.; Di Cairano, S.; Laughman, C.R.; Bortoff, S.A.

TR2018-026 February 2018

Abstract

In this chapter, a model predictive controller is designed for a multizone vapor compression system. Controller requirements representing desired performance of production-scale equipment are provided and include baseline requirements common in control literature (constraint enforcement, reference tracking, disturbance rejection) and also extended requirements necessary for commercial application (selectively deactivating zones, implementable on embedded processors with limited memory/computation, compatibility with demand response events.). A controller architecture is presented based on model predictive control to meet the requirements. Experiments are presented validating constraint enforcement and automatic deactivation of zones.

Intelligent Building Control

This work may not be copied or reproduced in whole or in part for any commercial purpose. Permission to copy in whole or in part without payment of fee is granted for nonprofit educational and research purposes provided that all such whole or partial copies include the following: a notice that such copying is by permission of Mitsubishi Electric Research Laboratories, Inc.; an acknowledgment of the authors and individual contributions to the work; and all applicable portions of the copyright notice. Copying, reproduction, or republishing for any other purpose shall require a license with payment of fee to Mitsubishi Electric Research Laboratories, Inc. All rights reserved.

Model Predictive Control of Vapor Compression Systems

Daniel J. Burns, Claus Danielson, Stefano Di Cairano, Christopher R. Laughman,
Scott A. Bortoff

Abstract In this chapter, a model predictive controller is designed for a multi-zone vapor compression system. Controller requirements representing desired performance of production-scale equipment are provided and include baseline requirements common in control literature (constraint enforcement, reference tracking, disturbance rejection) and also extended requirements necessary for commercial application (selectively deactivating zones, implementable on embedded processors with limited memory/computation, compatibility with demand response events.). A controller architecture is presented based on model predictive control to meet the requirements. Experiments are presented validating constraint enforcement and automatic deactivation of zones.

Notation

\mathbb{R} and \mathbb{Z} denote the set of real and integer numbers, respectively. The vector formed by concatenating $x \in \mathbb{R}^n$ and $y \in \mathbb{R}^m$ is denoted by $\text{col}(x, y) \in \mathbb{R}^{n+m}$. $I \in \mathbb{R}^{n \times n}$ and $0 \in \mathbb{R}^{n \times m}$ denote the identity and the all-zero matrices of appropriate dimension n and m , respectively. Inequalities are component-wise, and \prec and \succ (\preceq and \succeq) indicate positive and negative (semi)definiteness. A continuous-time signal $x(\tau)$ sampled with period T_s is denoted by the discrete-time signal $x(t) = x(tT_s)$ where $t \in \mathbb{Z}$. $x_{k|t}$ denotes the k -steps predicted value of x at time t .

D. J. Burns, C. Danielson, S. Di Cairano, C. R. Laughman, and S. A. Bortoff
Mitsubishi Electric Research Laboratories, 201 Broadway, Cambridge, MA, USA.
e-mail: {burns, danielson, dicarano, laughman, bortoff}@merl.com

1 Introduction

After more than 100 years of evolution, vapor compression systems (VCS) are now the most common means for commercial and residential space cooling [1], often employed for space or water heating [2], and extensively used in refrigeration (both stationary and mobile [3, 4]), desalination [5, 6], and cryogenic applications [7]. As discussed in Chapter 4, whereas early systems typically used fixed-speed compressors and fans, capillary tubes, and single condensers and evaporators, modern systems use state-of-the-art technology such as variable-speed compressors and fans, electronically-positioned expansion valves, and multiple heat exchangers operating in independent zones [8,9]. These machines must operate reliably in heating or cooling modes, over a broad range of operating conditions and climates for many years.

One effect of the advances in cycle technology is the increasing sophistication of the control systems [10–12]. Control strategies in early products were simple because of on/off actuation, limited sensing, and limited performance requirements such as zone temperature regulation [13, 14]. Efficiency requirements were met by designing the refrigeration cycle for a narrow set of conditions, and could be accomplished outside the scope of the control system design. However, modern VCS control systems must accommodate a broader set of requirements, including (1) maximizing energy efficiency over a broad range of operating conditions, (2) enforcing equipment protection constraints such as ensuring critical temperatures and pressures remain within permissible operating limits, (3) providing rapid transient response, (4) activation or deactivation of individual zones, and (5) integrating with intelligent building control strategies that periodically demand reduced energy consumption.

Model predictive control (MPC) is a strategy for the control of multivariable plants that satisfies many of these requirements explicitly, especially enforcement of plant input (actuator) and output (measurement) constraints with guarantees on stability and performance [15–17]. In MPC, control variables are computed by solving a constrained optimization problem in real-time that includes the predicted response of the system, resulting in a controller that achieves optimal performance according to specified objective function and enforces constraints on actuators and plant outputs. Furthermore, the MPC approach offers advantages related to the requirement of turning zones on and off, which can be met in a straightforward and scalable manner: the objective function and constraints can be changed online when a zone is activated, for example, altering the number of control objectives and decision variables in the associated optimal control problem [18–20]. Moreover, tuning the terms of the objective function is intuitive and leads to predictable performance and constraints can be modified or added during the design process while preserving system stability properties, eliminating the need for extensive revalidation during the product development. For the manufacturer, MPC thus provides an attractive strategy to meet a diverse set of requirements in a rigorous manner.

In this chapter, an MPC design for a VCS is presented. The design is offset-free to account for low-frequency model uncertainty and a state estimator in order to

estimate variables not directly measured [21, 22]. In contrast with other offset-free methods [23], this approach does not require fitting an input disturbance model—a task that is difficult because some disturbances, specifically the heat load, are unmeasured and possess significant uncertainty especially at low frequencies. The design enforces hard constraints associated with actuator limits and rate limits, and also enforces several output limits including a maximum compressor temperature, a minimum compressor discharge superheat temperature, and maximum and minimum heat exchanger temperatures. In addition, the control architecture provides for a separation of design concerns: distinct tuning parameters are provided to adjust the system for energy efficiency, constraint enforcement and transient performance, and these parameters are not coupled—enabling intuitive tuning.

The chapter is organized as follows. Section 2 describes the vapor compression system under consideration, derives a linear model and introduces pertinent constraints. Section 3 discusses the prioritized set of control system requirements and the strategy employed to meet them. In Section 4, an MPC design is presented including prediction model augmentations and Kalman filter derivation. Also in this section, an HVAC laboratory and validation experiments are described. Section 5 describes how the proposed control strategy meets extended requirements by describing a method that permits individual zones to be turned on or off within the MPC framework, and discusses optimization algorithms appropriate for low power embedded processors. Finally, concluding remarks are offered in Section 6.

2 Vapor Compression System Description

This section describes the dynamics and constraints of the multi-evaporator vapor compression system (ME-VCS) shown in Fig. 1. We treat the single evaporator system as a special case of the ME-VCS. The specific vapor compression system considered here is an air conditioner operating in cooling mode, and therefore the objects of conditioning are indoor volumes of air, although other applications of vapor compression systems can be considered (heat pumps, chillers, refrigeration systems, etc.) with straightforward substitutions of machine endpoints.

2.1 ME-VCS Dynamics

Consider the multi-zone vapor compression system operating in cooling mode shown schematically in Fig. 1. The ME-VCS is comprised of a single outdoor unit and N indoor units. The purpose of this system is to move both sensible and latent heat from the indoor zones to the outdoor air. When operating in cooling mode, the outdoor unit receives low pressure, low temperature refrigerant in the vapor state from the indoor units. The compressor performs work to increase the pressure and temperature of the refrigerant. The amount of work done is controlled by the com-

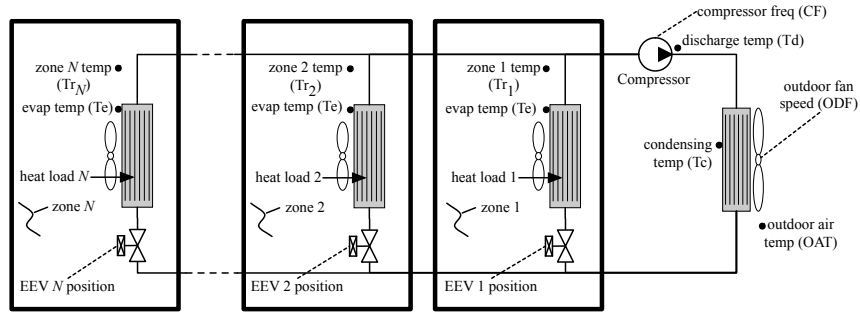


Fig. 1 Refrigerant piping arrangement of a multi-evaporator vapor compression system. The main actuators in the system are (i) the compressor, (ii) the outdoor (condenser) fan (ODF), and (iii) N electronic expansion valves (EEV). Sensors provide measurements of the compressor discharge temperature (T_d), the evaporating temperature (T_e), the condensing temperature (T_c) and the zone temperatures (Tr_i).

pressor rotational frequency CF . A sensor measures the discharge temperature T_d of the refrigerant leaving the compressor. The refrigerant then flows through the outdoor heat exchanger across which a fan forces air. Heat is transferred from the refrigerant causing it to condense from a vapor to a saturated liquid where the amount of heat removed from the refrigerant depends on the outdoor air temperature OAT and outdoor fan speed ODF . In cooling mode, the outdoor unit heat exchanger acts as a condenser, and the small pressure drop over the length of the heat exchanger enables the modeling assumption that the phase change of the refrigerant is approximately isobaric and occurs at a nearly constant condensing temperature T_c , which is measured by a sensor on the heat exchanger.

High pressure liquid refrigerant from the outdoor unit is then routed to the indoor units, indexed by $i \in \mathcal{I} = \{1, \dots, N\}$. The amount of refrigerant that enters the indoor unit is controlled by the opening position EEV_i of an electronic expansion valve. If the electronic expansion valve is open ($EEV_i > 0$), then refrigerant flows into the i -th indoor unit. As the refrigerant flows through the expansion valve, it undergoes an isenthalpic drop in pressure and temperature and changes state into a two-phase mixture of liquid and vapor. The low temperature two-phase refrigerant then flows through the indoor unit heat exchanger. An indoor fan forces air from the zone across the heat exchanger, which absorbs heat from the zone. An unmeasured heat load acts in each zone. The temperature of each zone Tr_i is measured in the return air stream. The heat absorbed by each indoor unit causes the refrigerant to evaporate from a two-phase mixture to a saturated vapor, so that these heat exchangers function as evaporators. As was also the case with the condenser, the small pressure drop over the length of the heat exchanger enables the modeling assumption of isobaric phase change that occurs at a nearly constant evaporating temperature T_e and is measured by sensors on the indoor unit heat exchangers. There are no measurements of refrigerant pressures or flow rates [24].

As discussed in Chapter 4, the dynamics of the ME-VCS can be modeled by a set of nonlinear differential-algebraic equations (DAEs)

$$0 = f(\dot{\phi}, \phi, u, v, d), \quad (1a)$$

$$y = h(\phi, u, v), \quad (1b)$$

where $\phi \in \mathbb{R}^n$ are the states representing thermofluid variables, $u \in \mathbb{R}^m$ are the control inputs, $v \in \mathbb{R}^l$ are the measured disturbances, $d \in \mathbb{R}^q$ are the unmeasured disturbances and $y \in \mathbb{R}^p$ are the measured outputs. These equations can be derived from the principles of fluid mechanics and thermodynamics, and typically involve spatial discretization of one-dimensional Navier-Stokes equations and empirically-determined closure relationships, including heat transfer correlations and frictional pressure drops [25, 26].

Generally speaking, Equation (1) is nonlinear, high-order ($n \approx O(100 - 1000)$), stiff, and marginally stable. Nonlinearity arises from thermofluid properties, the closure relations, and the mass, momentum and energy balance equations governing fluid dynamics and heat transfer [27]. The order can be high because of finite element or finite volume modeling methodologies which are required for practical reasons to accurately capture the spatial and temporal dynamics of the heat exchangers over a broad range of operating conditions [28]. Time scales can range from approximately 1 second for the fastest dynamics associated with pressure within the ME-VCS to as much as 1 week for the slowest timescale associated with heat transfer to the building envelope. This slowest time scale is inherent in (1) because we consider the zone air temperatures Tr_i to be among the measured outputs.

Idealized energy balance models of zone air thermodynamics assume an adiabatic process (no thermal losses to the environment), leading to an integrator in the equation for zone temperature dynamics. Physically, this marginal instability manifests as a diverging zone temperature whenever the cooling provided by the ME-VCS is not matched to the load in steady state. However, real systems are characterized by finite heat loads and non-adiabatic volumes and therefore the zone air temperature will ultimately reach some equilibrium, but this equilibrium is unknown and with the unmeasured load, contributes to uncertainty at low frequencies. Uncertainty in this context is used informally to mean that is difficult to experimentally calibrate or validate an instance of the model, and also that (1) is assumed to contain uncertainty in order to cover a diverse range of buildings in which a ME-VCS is installed and operated. The low frequency uncertainty implies that it is practically impossible to precisely compute the equilibrium $0 = f(0, \bar{\phi}, \bar{u}, \bar{v}, \bar{d})$ and the algebraic relationship among $\bar{\phi}$, \bar{u} , \bar{v} and \bar{d} for any model instance. This recognition is important to the architecture of any feedback compensator that aims to regulate the zone temperature to a setpoint with zero steady state error.

Fortunately, the dynamic response of the system in the “medium frequency” range of interest to the control system designer is remarkably linear and low order. To support this assertion, consider the data shown in Figure 2 where a vapor compression system is perturbed from three equilibrium points in order to characterize the sensitivity of nonlinearities to operating condition. The range of heat loads are

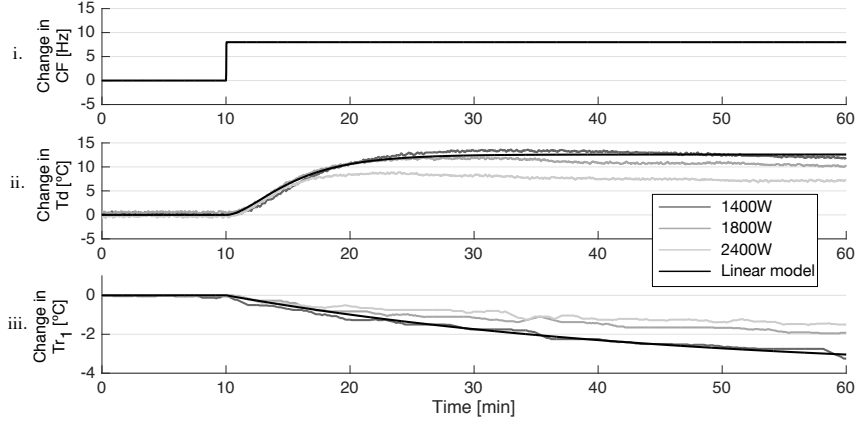


Fig. 2 Experiments in which compressor steps are applied at three different equilibrium points demonstrate that ME-VCS dynamics are well approximated by linear low-order models.

selected to cover from 50% to 85% of the rated capacity of this particular system. For each heat load, the compressor speed input is increased by 8 Hz, and the resulting responses of the compressor discharge temperature and the zone air temperature are shown. Despite settling to different values at steady state, the time constants for both outputs at each heat load are similar. For the systems considered, a medium frequency range of approximately 0.001 - 0.1 rad/s (corresponding to time scales of approximately 1 minute to 60 minutes) have been shown to be well approximated by low-order linear models. Feedback is employed to compensate the low-frequency uncertainty. This empirical observation enables the use of linear MPC.

Accordingly, the ME-VCS outdoor unit is modeled by

$$x_0(t+1) = A_{00}x_0(t) + \sum_{j=0}^N B_{0j}u_j(t) \quad (2a)$$

$$y_0(t) = C_{00}x_0(t) + w_0(t) \quad (2b)$$

where the inputs $u_0 = \text{col}(\text{CF}, \text{ODF}) \in \mathbb{R}^{m_0}$ are the compressor frequency CF and outdoor fan speed ODF, and the outputs $y_0 = \text{col}(\text{Td}, \text{Te}, \text{Tc})$ are the discharge Td, evaporator Te, and condenser Tc temperatures. The inputs u_j , $j = 1, \dots, N$ pertain to the individual indoor units and are described below. The model is fit to experimentally-obtained input-output data, and thus the state of the outdoor unit $x_0(t) \in \mathbb{R}^{n_0}$ is non-physical. The discrete-time model (2) describes the ME-VCS system when sampled with a period of 1 minute.

An additive output disturbance $w_0(t)$ is used to capture the effects of outdoor air temperature OAT on the measured outputs $y_0(t)$. Since the outdoor air temperature varies slowly with a diurnal period, we treat the disturbance $w_0(t)$ as constant on the time scale of the model (2),

$$w_0(t+1) = w_0(t). \quad (2c)$$

Remark 1. The entire ME-VCS is characterized by a single evaporating temperature due to the arrangement of valves shown in Fig. 1. In particular, the ME-VCS considered does not have valves at the outlet of each indoor unit. Thus, all indoor units with open valves operate at the same pressure and therefore the same evaporating temperature. As a consequence, the evaporator temperature T_e is modeled as an output of the outdoor unit (2b) and depends only on the state x_0 of the outdoor unit.

□

Over its range operation, the effect of the electronic expansion valve position EEV_i on the room temperature Tr_i is nonlinear. Therefore, each indoor unit has an inner feedback loop that manipulates the expansion valve position EEV_i to achieve a desired cooling capacity CC_i . The cooling capacity is the amount of heat removed from the zone by the corresponding evaporator per unit time. The cooling capacity controllers linearize the response from the reference cooling capacity command of each zone CC_i to the associated zone temperature Tr_i . Additional details on the inner feedback loops are provided in [29].

The i -th indoor unit, $i = 1, \dots, N$, is modeled by

$$x_i(t+1) = A_{ii}x_i(t) + A_{i0}x_0(t) + \sum_{j=0}^N B_{ij}u_j(t) \quad (2d)$$

$$y_i(t) = C_{ii}x_i(t) + w_i(t) \quad (2e)$$

where the input $u_i = CC_i \in \mathbb{R}^{m_i}$ is the cooling capacity command (which also appears in (2)) and the output $y_i = Tr_i \in \mathbb{R}$ is the zone temperature. The state of the i -th indoor unit $x_i \in \mathbb{R}^{n_i}$ is non-physical. The dynamics of the indoor unit depend on the state x_0 and input u_0 of the outdoor unit, as well as the inputs u_i for $i = 1, \dots, N$ for each of the indoor units.

Note that in some formulations, the indoor fan speed IDF_i may be considered as a control input and included in the definition of $u_i(t)$. However, in this application we permit the occupants to set the IDF for comfort reasons and therefore we treat the IDF as a measured disturbance. Because the IDF is measured, its effect on the zone temperature $y_i(t)$ can either be modeled as an input disturbance (in which case a dynamic model must be created that describes how changes in this input influence the measurements) or as an output disturbance (in which case only the steady state offset in zone temperature due to this disturbance is captured). Because the IDF is anticipated to change infrequently and therefore not excite the system dynamics, the output disturbance method is chosen. Additionally, the effects of the unmeasured heat load Q_i on the zone temperature is also modeled as an output disturbance. These are lumped into the term $w_i(t)$, assumed constant, and added to the output in (2e).

$$w_i(t+1) = w_i(t). \quad (2f)$$

It is convenient to gather both the outdoor (2a)–(2c) and indoor (2d)–(2f) models into a single representation

Table 1 Definition of Physical Signals

| Type | Symbol | Description | Units |
|------------------|--------|---|--------------------|
| Control Inputs | u_0 | Compressor Frequency (CF) Outdoor Fan Speed (ODF) | Hz rpm |
| | u_i | Cooling Capacity for i -th Zone (CC_i) | % |
| Measured Outputs | y_0 | Discharge Temp (T_d) | $^{\circ}\text{C}$ |
| | | Evaporating Temp (T_e) | $^{\circ}\text{C}$ |
| | | Condensing Temp (T_c) | $^{\circ}\text{C}$ |
| | y_i | i -th Zone Temp (Tr_i) | $^{\circ}\text{C}$ |
| Disturbances | w_0 | Temp offset due to Outdoor Air Temp (OAT) | $^{\circ}\text{C}$ |
| | w_i | Temp offset due to heat load (Q_i) and indoor fan speed (IDF $_i$) in i -th Zone | $^{\circ}\text{C}$ |

$$x(t+1) = Ax(t) + Bu(t) \quad (3a)$$

$$w(t+1) = Iw(t) \quad (3b)$$

$$y(t) = Cx(t) + Iw(t) \quad (3c)$$

where $x = \text{col}(x_0, x_1, \dots, x_N)$, $w = \text{col}(w_0, w_1, \dots, w_N)$, $u = \text{col}(\text{CF}, \text{ODF}, \text{CC}_i)$, $y = \text{col}(T_d, T_e, T_c, Tr_i)$, I is the identity matrix, and (A, B, C) are assembled as indicated in (2).

The models (2) and (3) are experimentally identified with the structure described above for the ME-VCS operating under typical conditions. The models (2) and (3) are a minimal realization of the dynamics of the ME-VCS, and the pairs (A_{ii}, B_{ii}) and (A_{ii}, C_{ii}) are controllable and observable, respectively, for $i = 0, \dots, N$. The signals $u_i(t)$, $y_i(t)$, and $w_i(t)$ for $i \in \mathcal{S}_0 = \{0, \dots, N\}$ are the deviations of the inputs, outputs, and disturbance from their nominal values, respectively. The physical meaning of the control inputs, measured outputs, and disturbances are summarized in Table 1.

2.2 ME-VCS Constraints

This section describes the constraints on outputs, states, and inputs of the multi-evaporator vapor compression system.

The outdoor unit measurements $y_0(t)$ of the discharge, evaporating and condensing temperatures are constrained to protect the equipment. Physical damage to the compressor motor can occur when its internal temperature exceeds some critical value, thus we have an upper-bound $T_{d_{\max}}$ on the compressor discharge temperature $T_d \leq T_{d_{\max}}$. If the indoor unit evaporators become too cold, frost can accumulate on the heat exchanger inhibiting heat transfer, thus we have a lower-bound $T_{e_{\min}}$ on the evaporating temperature $T_e \geq T_{e_{\min}}$. Additionally, excessive condenser-side pressures (as measured through the surrogate condensing temperature) can rupture components of the equipment, and thus we have an upper-bound $T_{c_{\max}}$ on the con-

denser temperature $T_c \leq T_{c_{\max}}$. Finally, to prevent the ingestion of damaging liquid refrigerant into the compressor, we define the refrigerant superheat temperature *at the compressor discharge port* T_{dsh} as an algebraic combination of other measurements $T_{dsh} = T_d - T_c$ and impose a lower-bound $T_{dsh_{\min}}$ on the discharge superheat temperature $T_{dsh} \geq T_{dsh_{\min}}$.

Note that the output constraints only apply to the outputs (or algebraic combinations thereof) (2b) of the outdoor unit. The outputs (2e) of the indoor units are unconstrained. In particular, the evaporating temperature constraint, which physically relates to the indoor units, is modeled as an output of the outdoor unit for reasons described in Remark 1.

The outdoor unit has lower and upper bounds on the compressor frequency $CF_{\min} \leq CF \leq CF_{\max}(t)$ and outdoor fan speed $ODF_{\min} \leq ODF \leq ODF_{\max}$. Furthermore, we allow $CF_{\max}(t)$ to be time-varying to accommodate the action of external protection logic, or as a means to implement building-level demand response.

Since the cooling capacity commands represent a fraction of the total rated capacity of each evaporator [29], the inputs to the indoor unit capacity controllers have lower and upper bounds $CC_{i,\min} \leq CC_i \leq CC_{i,\max}$. The actuator constraints associated with the electronic expansion valves EEV_i are enforced within the indoor unit capacity controllers.

The system also has constraints on the amount the inputs can change during each sample period. The outdoor unit has constraints on the change in compressor frequency $\Delta CF_{\min} \leq \Delta CF \leq \Delta CF_{\max}$ and outdoor fan speed $\Delta ODF_{\min} \leq \Delta ODF \leq \Delta ODF_{\max}$.

The indoor units have inner feedback loops that control the position of the electronic expansion valves to track the cooling capacity command. The change in cooling capacity command is bounded $\Delta CC_{i,\min} \leq \Delta CC_i \leq \Delta CC_{i,\max}$ to ensure that the transient response of the inner-loop controllers settles during the sample period.

3 Control Requirements

The control requirements for a production-grade vapor compression system extend beyond temperature regulation. The ME-VCS must also protect itself from damage, permit some zones to shut off while others remain in service, minimize energy consumption to the extent possible and accomplish these objectives while operating over a wide and variable range of outdoor and load conditions. Additionally, emerging trends in building efficiency standards, smart grid compatibility and tighter integration with other HVAC equipment require flexibility in the control method to, for example, adapt the operation of the machine to a demand response event or cooperate with other equipment such as dedicated ventilation systems to efficiently manage sensible and latent loads. Finally, economic and reliability pressures demand the use of a limited number of low-cost sensors and low-end embedded processors.

The following is a prioritized list of control objectives that is divided into two parts: baseline requirements and extended requirements. The baseline requirements

are control objectives for the system during nominal operating modes and include constraint enforcement, disturbance rejection and transient response metrics. The extended requirements address practical concerns often neglected in the literature such as compatibility with startup, shutdown, equipment protection and defrost logic, response to building management system requests for energy reduction, and the ability to shut off some zones.

3.1 Baseline Controller Requirements

This section lists control requirements for baseline operation of the ME-VCS. Here “baseline operation” refers to the system operating around an equilibrium state.

- B.1 Constraint Enforcement** The controller should enforce the input (actuator), input rate and output constraints described in Section 2.2.
- B.2 Setpoint Regulation** If B.1 is satisfied, the controller should drive each zone air temperature to its setpoint with zero steady state error.
- B.3 Disturbance Rejection** The controller should achieve B.2 given changes in heat loads and outdoor air temperatures.
- B.4 Energy Minimization** If B.1–B.3 are satisfied, the controller should drive the system to energy-optimal operating points in steady state. Note that energy performance is not defined during transients.
- B.5 Transient Performance** Ensuring B.1 is satisfied, the controller should minimize the time required to adjust to a new setpoint with an overshoot of less than 1°C. The response time is left unspecified because it depends on (i) whether the setpoint change is a step-up or step-down, (ii) the unknown volume of air in the zone and (iii) the unmeasured load.

3.2 Extended Controller Requirements

In addition to the baseline requirements, the controller must also meet the following extended requirements:

- E.1 Permit individual zones to be shut off** Often low heat loads in some zones or occupant desires are such that some evaporators must be turned off while others remain in service. The control system should enable this type of behavior.
- E.2 Computationally tractable** Embedded processors are often limited in processing ability, memory availability and communication speeds. The algorithmic realization of the controller should be conformable to such computational platforms.
- E.3 Compatible with Demand Response** The controller should adapt its energy consumption in response to signals received from a Building Management System during a Demand Response event.

E.4 Independent parameter-to-performance metric relationship The parameters that adjust the behavior of the controller should independently and predictably do so. For example, a parameter that specifies an output constraint should not affect energy performance and the parameter that specifies energy performance should not affect the output constraints. Parameter independence enables late-stage modification of specifications without extensive re-validation, and therefore speeds product development.

3.3 Control Design Strategy

Our strategy to meet these requirements is outlined in this section, with additional details and controller derivations provided in Sections 4 and 5. Model Predictive Control (MPC) is selected as the main approach because (i) constraint enforcement is critical (B.1), (ii) a model (3) of the process dynamics is available and a prediction model for the references can be created, and (iii) control invariant sets and online updates to the cost function enable satisfaction of the extended requirements.

An outline of the design process for model predictive control is shown in Fig. 3. Designing a model predictive controller requires specifying a receding horizon optimal control problem in a series of offline steps. Briefly, starting from a model of the ME-VCS dynamics, augmentations to the model are performed to meet controller requirements, resulting in a prediction model that achieves desired closed-loop dynamics. The prediction model is used in the specification of the optimal control problem and as the basis of a online state estimator. The controller requirements are also used to specify the cost function and constraint components of the optimal control problem. A control problem with quadratic cost and linear constraints is equivalent to a constrained quadratic program that is solved online by an optimization algorithm [30].

The following describes how we apply the MPC design framework of Fig. 3 to meet the control requirements. Specifically, and in order of priority, the constraint enforcement requirement (B.1) is satisfied through appropriate specification of the constraints in the optimal control problem. Zone temperature regulation (B.2) is addressed by specifying a setpoint temperature for each zone and penalizing tracking errors in the cost function. Disturbance rejection (B.3) is addressed with output disturbance models incorporated and the use of integral action on the zone temperature tracking errors. A Kalman filter is used to estimate unmeasured states that are used to initialize the prediction model.

To address the requirement to minimize energy consumption (B.4), we note that the number of actuators is greater than the number of zones, which implies that sufficient degrees-of-freedom exist to regulate an additional variable while simultaneously meeting zone temperature setpoint objectives, and we therefore introduce another reference correlated to steady state thermodynamic efficiency. While many control approaches for vapor compression systems regulate evaporator superheat as a surrogate for efficiency, we instead select the compressor discharge temperature

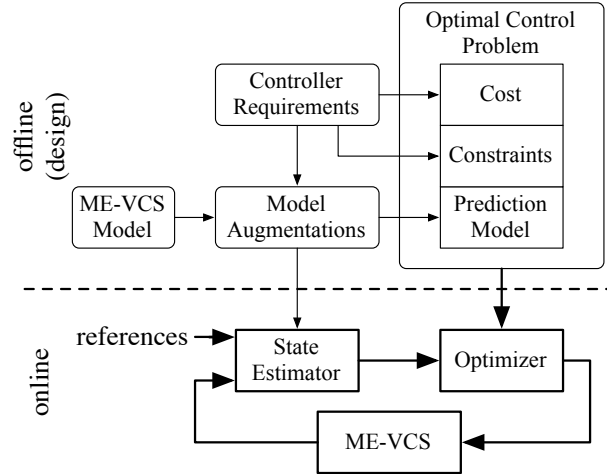


Fig. 3 A model predictive controller is designed in a series of offline steps to specify an optimal control problem. Controller requirements inform the creation of the cost function, constraints, and the model augmentations needed create the prediction model. The optimal control problem is then converted into a representation suitable for online calculation of the control action.

T_d because it is measured and because the steady state power consumption at any operating point is convex with respect to it [31, 32]. Therefore, energy-optimal values of T_d are used to create a reference, and tracking errors of this reference are penalized in the cost function.

After introducing the T_d reference there still remains an additional degree-of-freedom. However, it is more important to enforce constraints, especially through transients, than to regulate an additional process variable. We therefore choose to use the additional degree-of-freedom to provide flexibility to the optimizer to meet the constraints. The transient performance objective (B.5) is addressed through the selection of appropriate penalty terms in the cost function and the reliance on the actuator and output constraint enforcement to safely extract the high performance only obtained near equipment limits.

The extended controller requirements are addressed by exploiting properties of the MPC method. Selectively turning zones on or off (E.1) is accomplished with online modification to the penalty terms in the MPC cost function, effectively removing zone-level process variables and control inputs from the optimization problem. The manipulation of the controller cost function is performed when either an occupant specifies that a zone is to be shut off or supervisory logic determines that a zone should be deactivated. A detailed derivation of this approach and validation experiments are provided in Section 5.

By requirement (E.2), the realization of the online calculations method must be computationally tractable and fit within the limited memory available on low cost embedded systems. The reconfigurable MPC strategy for shutting off zones with

online modifications avoids the need to store individual controllers for every possible on/off configuration, and the relatively slow dynamics of (2) provide ample time between controller updates for advanced algorithms [16] to reliably solve the associated quadratic program.

The requirement of adapting to a demand response request (E.3) is enabled through the parameter independence property of our MPC design and therefore (E.3) is satisfied when (E.4) is satisfied. The controller derived in Sections 4 and 5 is shown to decouple the effect of one parameter from another. Not only does this property simplify tuning and validation, but it also provides tunable parameters that can be exposed to higher-level supervisory control systems such as with a building management system. For example, zone temperature set points, or the controller discharge reference or the maximum compressor frequency can each be dynamically adjusted by external logic to alter the energy consumption behavior without modifying, for example, the controller’s ability to enforce constraints.

As a result of the controller structure presented in the next section, the ability to meet the baseline requirements degrades gracefully and in accordance with the listed priority. We show this in experiments in the following section.

4 Model Predictive Control for Baseline Requirements

In this section, we show how a model predictive control strategy can be applied to meet the baseline requirements described in Section 3.1. The key elements of the control algorithm are described, including the prediction model used to define performance and constrained outputs, the Kalman Filter and the optimal control problem formulation. Finally, experiments are conducted to validate the approach.

A block diagram of the closed loop system is shown in Fig. 4. A state estimator which includes a Kalman Filter (plus additional functions for generating other states) receives zone temperature references $r_i(t)$, a signal $u_{0,\max}(t)$ indicating the time-varying maximum compressor speed from external control logic, the outputs $y(t)$ measured from the ME-VCS, and the control inputs $u(t)$ supplied to it, and computes estimated states $\bar{x}(t)$ of a prediction model. The model predictive controller uses $\bar{x}(t)$ to define and to solve a constrained optimal control problem to generate the control inputs $u(t)$.

4.1 Kalman Filter

The structure of the Kalman Filter is designed to satisfy the setpoint regulation requirement (B.2) and the disturbance rejection requirement (B.3), which demands that the states be estimated such that the outputs of the estimator \hat{y} match the measurements y at steady state when the disturbances are constant.

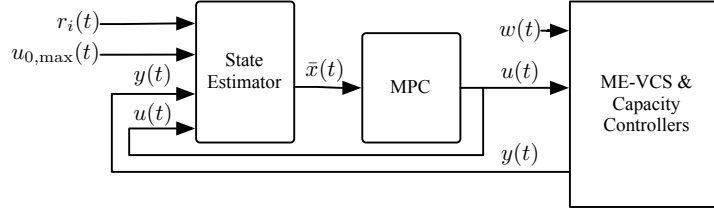


Fig. 4 Block diagram of the closed loop system.

Starting from model (3), we construct the Kalman Filter for the ME-VCS plant dynamics

$$\hat{x}(k+1) = A\hat{x}(k) + Bu(k) + L_x(y(k) - \hat{y}(k)) \quad (4a)$$

$$\hat{w}(k+1) = \hat{w}(k) + L_w(y(k) - \hat{y}(k)) \quad (4b)$$

$$\hat{y}(k) = C\hat{x}(k) + \hat{w}. \quad (4c)$$

The estimator gain matrix $L = [L_x \ L_w]$ can be computed using conventional methods such as minimizing an H_2 norm.

In addition to the estimated states $[\hat{x}^T \ \hat{w}^T]^T$, there are additional variables required by the MPC that are added to the state vector, resulting in the augmented state vector \bar{x} . The block labeled “State Estimator” in Fig. 4 contains the Kalman Filter (4) which computes $[\hat{x}^T \ \hat{w}^T]^T$, and also other equations for computing the remaining components of \bar{x} , as described in the next section.

4.2 Prediction Model Augmentations

In this section, we begin with the plant model (3) and augment the dynamics to define performance outputs and constrained outputs for the optimal control problem. Each augmentation is performed to meet one or more control requirements, as will be indicated.

Augmentation 1 (Incremental Inputs) *Because there are constraints on both the magnitude of the inputs and the amount they can change at each sample period, we redefine the inputs of (3) to explicitly track the incremental control action [33]. Let $u(t) = u(t-1) + \Delta u(t)$, define the actuator state $x_u(t) := u(t-1)$ and augment the state in (3) with x_u . Finally, augment the constrained outputs with this new state so that the magnitude of the control inputs can be constrained, satisfying B.1.*

Augmentation 2 (Time-varying Constraints) *In order to be compatible with demand response commands (E.4), we allow the maximum compressor maximum frequency constraint to be time-varying $u_{0,max}(t) = CF_{max}(t)$. Therefore, we want to enforce $CF(t) \leq CF_{max}(t)$ so we rewrite the constraint as $CF(k) - CF_{max}(t) \leq 0$*

and define the new constrained output $y_{iv}(t) := CF(t) - CF_{max}(t)$ where the subscript is meant to indicate a time-varying constraint. This new constraint will have a maximum value of 0, which ensures that CF remains less than the constrained value.

Because the value of CF_{max} comes from an external source, we define a new state $x_{iv}(t) := CF_{max}(t)$ and include it in the definition of the prediction model state. The dynamics of this exogenous constraint cannot be predicted, so we assume that it is constant $x_{iv}(t+1) = x_{iv}(t)$.

Note that allowing a building management system to specify the maximum compressor speed permits a more direct influence over the vapor compression system's energy consumption than traditional means where zone temperature setpoints are adjusted with offsets.

Augmentation 3 (References and Performance Outputs) The baseline requirements include setpoint regulation (B.1) of the zone air temperatures and energy minimization (B.4) in steady state. To achieve both requirements, we first introduce the references into the prediction model, then define the performance outputs as the tracking errors and integrals thereof.

The energy-optimal discharge temperature reference is a linear function of the compressor frequency CF (control input) and the outdoor air temperature OAT (disturbance input) [34] given by

$$r_0 = F_{00}u_0 + G_{00}w_0 \quad (5)$$

where the coefficients F_{00}, G_{00} are experimentally characterized to minimize power consumption over a range of operating conditions. Since w_0 is assumed constant over the timescale of the model (3), the prediction model of the reference discharge temperature is given by

$$r_0(t+1) = r_0(t) + F_{00}\Delta u_0(t). \quad (6)$$

The reference zone temperatures are assumed constant and modeled by

$$r_i(t+1) = r_i(t), \quad (7)$$

for $i = 1, \dots, N$. For consistency we define $F_{ii} = 0$ and $G_{ii} = 0$ for $i = 1, \dots, N$. Thus, the composite reference $r = \text{col}(r_0, r_1, \dots, r_N)$ is modeled by

$$r(t+1) = r(t) + F\Delta u_0(t)$$

where $F = \text{col}(F_{00}, F_{11}, \dots, F_{NN})$ and $G = \text{col}(G_{00}, G_{11}, \dots, G_{NN})$. The prediction model state vector is then augmented to include these references.

Using these references, tracking errors are computed for the compressor discharge temperature and the zone temperatures

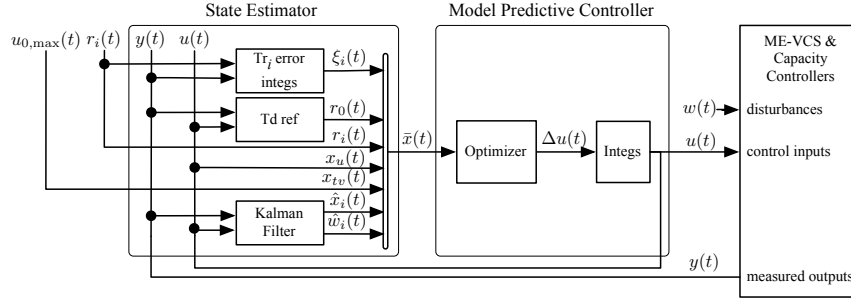


Fig. 5 Controller block diagram. A state estimator computes the states defined by the prediction model from zone integrators, the Td reference function and the Kalman Filter. An optimizer solves the constrained optimal control problem to determine incremental input vales that are integrated to generate the control inputs.

$$e_0(t) = Td - r_0(t) \quad (8)$$

$$e_i(t) = Tr_i(t) - r_i(t) \quad i = 1, \dots, N \quad (9)$$

Additionally, the zone temperature tracking errors are integrated

$$\xi_i(t+1) = \xi_i(t) + e_i(t) \quad i = 1, \dots, N \quad (10)$$

The zone temperature error integrators (10) provide integral action and hence zero steady-state tracking error in the presence of uncertainties in zone air volume and heat loads. Although the auxiliary output offset (2c) and (2f) provide offset-free tracking [35, 36], our experimental results have shown that combining both integral action and output offsets provides improved transient performance.

Finally, the performance outputs \bar{z} are defined as the tracking errors and the integrals of the zone temperature tracking errors $\bar{z} := \text{col}(e_o, e_i, \xi_i)$, for $i = 1, \dots, N$.

The augmentations result in the prediction model

$$\bar{x}(t+1) = \bar{A}\bar{x}(t) + \bar{B}\Delta u(t) \quad (11)$$

$$\bar{y}(t) = \bar{C}\bar{x}(t) + \bar{D}\Delta u(t) \quad (12)$$

$$\bar{z}(t) = \bar{E}\bar{x}(t) \quad (13)$$

where $\bar{x} = \text{col}(\hat{x}(t), \hat{w}(t), r(t), \xi_i(t), x_{tv}(t), x_u(t))$, $i = 1, \dots, N$ are the augmented states, $\bar{y} = \text{col}(Td, Te, Tc, Tdsh, CF, ODF, CC_i, CF - CF_{max})$, $i = 1, \dots, N$ are the constrained outputs and $\bar{z} = \text{col}(Td - r_0, Tr_i - r_i, \xi_i)$, $i = 1, \dots, N$ are the performance outputs and $\Delta u = \text{col}(\Delta CF, \Delta ODF, \Delta CC_i)$, $i = 1, \dots, N$ are the inputs.

4.3 Optimal Control Problem Formulation

As shown in Fig. 5, at each sample time the estimator computes the augmented state $\bar{x}(t)$, and an optimizer computes the control input by solving the following constrained finite-time optimal control problem

$$\min_{\Delta \mathbf{u}} \quad \bar{x}'_{T|t} P \bar{x}_{T|t} + \sum_{k=0}^{T-1} \bar{z}'_{k|t} Q \bar{z}_{k|t} + \Delta u'_{k|t} R \Delta u_{k|t} \quad (14a)$$

$$\text{s.t.} \quad \bar{x}_{k+1|t} = \bar{A} \bar{x}_{k|t} + \bar{B} \Delta u_{k|t} \quad (14b)$$

$$\bar{y}_{k|t} = \bar{C} \bar{x}_{k|t} + \bar{D} \Delta u_{k|t} \quad (14c)$$

$$\bar{z}_{k|t} = \bar{E} \bar{x}_{k|t} \quad (14d)$$

$$\Delta u_{\min} \leq \Delta u_{k|t} \leq \Delta u_{\max} \quad (14e)$$

$$y_{\min} \leq \bar{y}_{k|t} \leq y_{\max} \quad (14f)$$

$$\bar{x}_{0|t} = \bar{x}(t). \quad (14g)$$

where $\bar{x}_{k|t}$ is the predicted augmented state under the incremental input $\Delta u_{k|t}$ over the finite prediction horizon of T -steps, and $\Delta \mathbf{u} = \text{col}(\Delta u_{0|t}, \dots, \Delta u_{T-1|t})$ is the optimization variable. The first element from $\Delta \mathbf{u}$ is selected from the solution to the optimization problem, $\Delta u(t) = \Delta u_{0|t}^*$ and because this variable is an incremental input (by Augmentation 1), the model predictive controller integrates the incremental input $\Delta u(t)$ (see Fig. 5) to obtain the implemented input

$$u(t) = u(t-1) + \Delta u_t \quad (15)$$

which is then applied the ME-VCS.

The cost function (14a) penalizes the predicted performance outputs $\bar{z}_{k|t}$ and incremental inputs $\Delta u_{k|t}$ over the prediction horizon, and the states at the end of the prediction horizon $\bar{x} + T|t$. The performance output $\bar{z}_0 = z_0 - r_0$ is the difference between the discharge temperature $z_0 = T_d$ and the reference discharge temperature $r_0 = T_{d,\text{ref}}$, which maximizes energy efficiency at steady state. Additional performance outputs $\bar{z}_i = \text{col}(z_i - r_i, \xi)$, $i = 1 \dots N$ relate to the N indoor units and include the room temperature tracking errors $z_i - r_i$, and their integrals ξ . The matrix $Q \geq 0$ is used to weigh the relative importance of the performance outputs. Changes in control inputs $\Delta u_{k|t}$ are also penalized, and the matrix $R > 0$ specifies their relative importance. The terminal state matrix $P > 0$ is designed to ensure that tracking errors are locally asymptotically stable, and may be computed by solving the Riccati equation with slight modifications as discussed in [37].

The optimal control problem (14) is converted to a quadratic program in an offline step [30] and parameters representing the quadratic program are stored for online calculation of the control action. An algorithm for solving the quadratic program (labeled ‘‘Optimizer’’ in Fig. 5) uses these parameters with the current instance of the augmented state \bar{x} to solve the control problem (14) on the embedded ME-VCS processor to compute Δu .

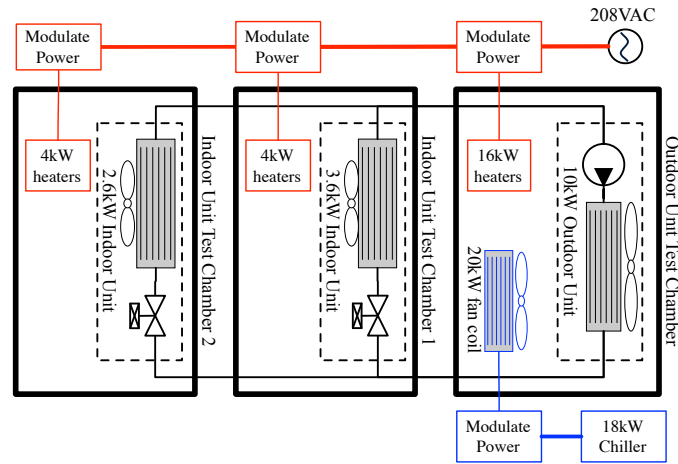


Fig. 6 The outdoor unit and two indoor units of a split-ductless style vapor compression system is installed in three test chambers. A balance-of-plant system consists of a set of adjustable-power heaters (red) and an adjustable-power hydronic system (blue), and is used to set the environmental conditions of the vapor compression system under test.

4.4 Experimental Validation

In this section, we present experiments demonstrating that the MPC design satisfies the baseline requirements. We begin by briefly describing the experimental testing facility, then show two experimental results aimed at validating the controller design.

The ME-VCS system is a commercially-available two-zone unit installed in a test facility that includes a balance-of-plant system to supply heating and cooling loads, as shown schematically in Fig. 6. The ME-VCS outdoor unit (consisting of the compressor, outdoor heat exchanger and fan, and EEVs) is installed in a 6.3 m^3 insulated test chamber and is connected via refrigerant lines to two indoor units (each consisting of indoor heat exchangers and fans), which are installed in separate 9.9 m^3 insulated test chambers. The balance-of-plant system consists of variable power heaters and a variable power chiller, hydronic fan coils and associated controllers and is configured to regulate the heat loads in the indoor unit test chambers and the air temperature in the outdoor unit test chamber.

The plant model (2) is derived from experimental data collected in this test facility as follows: With 1.6 kW fixed heat loads applied in the indoor unit test chambers, the outdoor test chamber regulated to 35°C , and the vapor compression system operating at steady state, steps are separately applied to each control input u (CF, ODF, CC_1 and CC_2). Measurements of the system outputs y are collected the data is used to fit a model of the plant in the form of Equation (2).

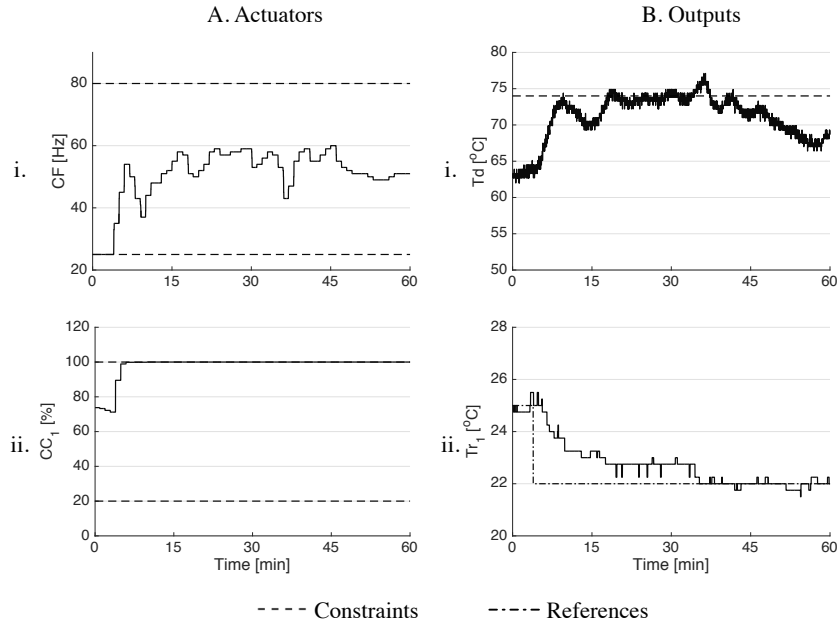


Fig. 7 A step down in the zone temperature setpoint causes the Td and capacity command constraints to become active.

4.4.1 Experiment 1: Enforcing Multiple Simultaneous Constraints

This section describes an experiment where a step change to a setpoint is applied in order to induce a transient response where an output constraint becomes active and thereby demonstrate enforcement (B.1).

Referring to Fig. 7, the vapor compression system is operated until steady state conditions are present with a zone setpoint $r_1 = 25^\circ\text{C}$ and the boundary conditions $Q_1 = 2200\text{ W}$, and $\text{OAT} = 35^\circ\text{C}$. At $t = 5\text{ min}$, the setpoint is lowered to $r_1 = 22^\circ\text{C}$ (Fig. 7B-ii), and the controller increases the CF and saturates CC_1 to reduce the temperature in that zone. As a result of the increased CF, the discharge temperature increases until it reaches its constraint at $t = 8\text{ min}$ (Fig. 7B-i). The CF commands (Fig. 7A-i) computed by the MPC maintain Td below its constraint. From $t = 20$ to 35 min. , Td largely follows the constraint until at $t = 35\text{ min}$ a constraint violation of about 2°C occurs (Fig. 7B-i), which is attributed to modeling errors. Additionally, the CC_1 input is also saturated at its maximum value (Fig. 7A-ii), making two constraints active during this transient. The Td constraint violation causes an immediate reduction in CF at $t = 35\text{ min}$, and Td is decreased accordingly, relieving the violation. Finally, zone 1 achieves the setpoint with zero steady state error at $t = 37\text{ min}$.

This experiment demonstrates that both input (actuator) and output (sensor) constraints can be simultaneously enforced by the MPC during transients, satisfying

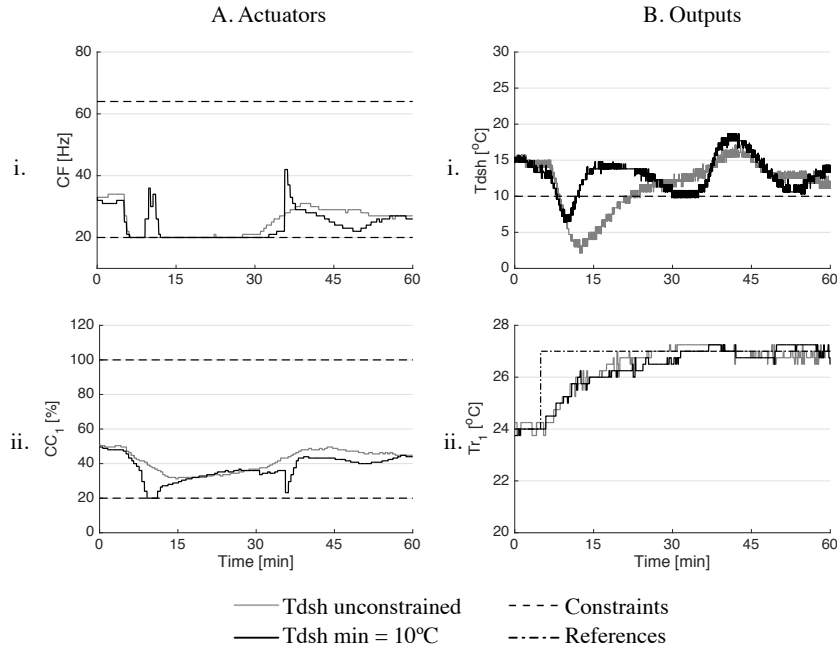


Fig. 8 The MPC controller raises the room temperature as quickly as possible, despite a constraint violation that slows the zone temperature response.

the constraint enforcement requirement (B.1). Additionally, because the maximum cooling capacity occurs at the constraints, the zone temperature response in Fig. 7B-ii represents the fastest pull-down in zone temperature possible from this system at these conditions, satisfying the transient performance requirement (B.5).

4.4.2 Experiment 2: Recovery from Constraint Violation

This section describes an experiment showing the controller meeting requirement priority. Specifically, transient performance (B.5) is reduced when a constraint becomes violated demonstrating that the controller alters behavior to prioritize constraint enforcement (B.1).

Referring to Fig. 8, two experiments are performed wherein an MPC that includes a T_{dsh_min} constraint (black lines) is compared to the same controller where T_{dsh} is unconstrained (gray lines). A zone temperature reference r_1 step up from 24°C to 27°C is applied at $t = 5$ min. (Fig. 8B.-ii) to cause a reduction in both the CF and CC_1 commands. Note that the capacity command can be intuitively understood as proportional to the associated expansion valve (i.e., when CC_1 is reduced, EEV_1 becomes more closed). This simultaneous reduction in both actuators causes the discharge superheat temperature T_{dsh} to fall rapidly, resulting in a constraint viola-

tion due to modeling errors. For the case where T_{dsh} is unconstrained (gray lines), the MPC acts to raise the zone temperature (Fig. 8B.-ii) as quickly as possible. The CF is reduced to its minimum constraint for the duration of the transient, and the capacity command is smoothly reduced in an effort for T_d to track its reference r_0 (not shown for clarity). Under these actuator commands, the room temperature first reaches the setpoint at about $t = 25$ min. But the violation for T_{dsh} is larger in this case.

In this experiment, the MPC controller with a $T_{dsh_{min}} = 10^\circ\text{C}$ constraint (black lines) selects actuator commands that reflect the prioritized baseline requirement list. In particular, actuator commands and the resulting room temperature response initially follow the same trajectories, but when the T_{dsh} constraint is violated at $t = 8$ min, the controller prioritizes recovery from the constraint violation at the penalty of increased time in meeting the setpoint. In particular, when T_{dsh} falls below the minimum value, the compressor frequency is rapidly increased and the expansion valve is simultaneously closed down, where both actions serve to increase T_{dsh} , but at a penalty of slower warming of the room. In this case, the room temperature first reaches the setpoint at $t = 31$ min, but T_{dsh} recovers quickly from the constraint violation.

5 Model Predictive Control for Extended Requirements

In this section, we expand on the MPC design in order to meet the extended controller requirements described in Section 3.2. We present a new method that permits reconfiguration of the model predictive controller to accommodate the changing number of control objectives and inputs when individual zones are turned on or off, and demonstrate the method in experiments. We also provide an overview of two optimization algorithms that are suitable for the embedded processors typically used in commercial HVAC equipment.

5.1 *Selectively Deactivating Zones with Reconfigurable MPC*

In practice, many multi-evaporator systems often experience low heat loads in zones such that the corresponding evaporator no longer needs to provide cooling and should be shut off while the remaining evaporators continue to operate. This function is captured in the extended controller requirement (E.1). Turning an indoor unit on or off alters the model of the plant dynamics, and therefore induces changes in the prediction model and number of regulated variables, actuators, sensors, and constraints. A structural change of this nature conventionally would require a separate controller for each machine configuration, where at each control cycle the appropriate controller is switched in at runtime [19, 20]. However this standard approach

is too memory intensive for the available embedded processor and violates requirement (E.2).

The reconfigurable MPC approach described here features a single “master” controller designed and tuned for the configuration where all subsystems are active, and enables automatic reconfiguration of the controller by simple operations for configurations when any number of evaporators are deactivated. In this way, the master controller is designed and tuned using a single appropriately-partitioned prediction model. The method scales to any combination of active evaporators in a multi-evaporator vapor compression system.

In this section, we briefly describe how the configuration-dependent prediction model is obtained and used to specify a reconfigurable optimal control problem. The terms in the cost function are then manipulated online based on the ME-VCS configuration to obtain an controller specific to the machine configuration. Finally, we show an experiment where the reconfigurable MPC autonomously activates and deactivates a zone due to low heat load conditions.

5.1.1 Configuration-Dependent Model

An indoor unit is said to be active when its associated expansion valve is open allowing refrigerant to flow through the evaporator providing cooling. Conversely, an indoor unit is said to be inactive when its associated expansion valve is closed and no cooling occurs. A configuration of the ME-VCS is a combination of active and inactive indoor units.

To each indoor unit $i \in \mathcal{I}$ we assign a configuration variable $\zeta_i \in \{0, 1\}$ where $\zeta_i = 1$ if the unit is active and $\zeta_i = 0$ if the unit is inactive. The configuration of the entire ME-VCS is given by the vector $\zeta = \text{col}(\zeta_0, \zeta_1, \dots, \zeta_N)$ where $\zeta_0 = 1$ since the outdoor unit is always active. The configuration $\zeta \in \{1\} \times \{0, 1\} \times \dots \times \{0, 1\}$ is used to obtain a parameter-dependent controller [38] which operates for any ME-VCS configuration. In the subsequent analysis, the configuration is assumed to be kept constant, at least for a sufficiently long dwell time.

For configuration ζ , the dynamics of the outdoor unit are modeled by

$$x_0(t+1) = A_{00}x_0(t) + \sum_{j=0}^N \zeta_j B_{0j} u_j(t) \quad (16a)$$

where the future state $x_0(t+1)$ of the outdoor unit is only affected by the inputs $u_j(t)$ of active units $\zeta_j = 1$. The dynamics of the i -th indoor unit are modeled by

$$x_i(t+1) = A_{ii}x_i(t) + \zeta_i A_{i0}x_0(t) + \sum_{j=0}^N \zeta_i \zeta_j B_{ij} u_j(t) \quad (16b)$$

If the i -th indoor unit is inactive $\zeta_i = 0$, then its future state $x_i(t+1)$ depends only on its current state $x_i(t)$. If the i -th indoor unit is active $\zeta_i = 1$, then its future state $x_i(t+1)$ also depends on the outdoor unit state $x_0(t)$ and the inputs $u_j(t)$ to the other active indoor units $\zeta_j = 1$.

The configuration-dependent model (16) can be written more compactly in the form

$$x(t+1) = A^\zeta x(t) + B^\zeta u(t) \quad (17)$$

where $x = \text{col}(x_0, x_1, \dots, x_N)$ and $u = \text{col}(u_0, u_1, \dots, u_N)$ are the composite state and input respectively. The state-update matrix A^ζ is block lower-arrowhead and the input matrix B^ζ is dense.

5.1.2 Configuration-Dependent Augmentations

In the design of the reconfigurable MPC, similar augmentations are made as described in Section 4.2 to create the prediction model. Here, we highlight the configuration-dependent augmentations. Specifically, the integrators of the zone temperature tracking errors are expressed in configuration-dependent form as

$$\xi_i(t+1) = \zeta_i \xi_i(t) + \zeta_i (e_i(t)). \quad (18)$$

And we define the state $x_{u,i}(t) = u_i(t-1)$. Note that when the i -th indoor unit is inactive $\zeta_i = 0$ the corresponding integrator is shut-off $\xi_i(t+1) = 0$. The incremental inputs are configuration-dependent

$$u_i(t) = \zeta_i u_i(t-1) + \zeta_i \Delta u_i(t) \quad (19)$$

Note that when the i -th indoor unit is inactive $\zeta_i = 0$ equation (19) sets the input $u_i(t)$ to zero, and the associated inner feedback loop fully closes the expansion valve.

The remaining augmentations are applied as in Section 4.2. The configuration-dependent prediction model then becomes

$$\bar{x}(t+1) = \bar{A}^\zeta \bar{x}(t) + \bar{B}^\zeta \Delta u(t) \quad (20a)$$

$$\bar{y}(t) = \bar{C}^\zeta \bar{x}(t) + \bar{D}^\zeta \Delta u(t) \quad (20b)$$

$$\bar{z}(t) = \bar{E}^\zeta \hat{x}(t) \quad (20c)$$

where $\bar{x} = \text{col}(\hat{x}_i(t), \hat{w}_i(t), r(t), \xi_i(t), x_{tv}(t), x_{u,i}(t)), i = 1, \dots, N$ are the augmented states, $\bar{y} = \text{col}(\text{Td}, \text{Te}, \text{Tc}, \text{Tdsh}, \text{CF}, \text{ODF}, \text{CC}_i, \text{CF} - \text{CF}_{max}), i = 1, \dots, N$ are the constrained outputs and $\bar{z} = \text{col}(\text{Td} - r_0, \text{Tr}_i - r_i, \xi_i), i = 1, \dots, N$ are the performance outputs and $\Delta u = \text{col}(\Delta \text{CF}, \Delta \text{ODF}, \Delta \text{CC}_i), i = 1, \dots, N$ are the inputs.

5.1.3 Configuration-Dependent Optimal Control Problem

The reconfigurable model predictive controller computes the control input by solving the following configuration-dependent finite-time optimal control problem

$$\min_{\Delta \mathbf{u}} \quad \sum_{i=0}^N \left(\zeta_i \bar{x}'_{i,T|t} P_i \bar{x}_{i,T|t} + \sum_{k=0}^{T-1} \zeta_i \bar{z}'_{i,k|t} Q_i \bar{z}_{i,k|t} + \lambda_i \Delta u'_{i,k|t} R_i \Delta u_{i,k|t} \right) \quad (21a)$$

$$\text{s.t.} \quad \bar{x}_{k+1|t} = \bar{A}^1 \bar{x}_{k|t} + \bar{B}^1 \Delta u_{k|t} \quad (21b)$$

$$\bar{y}_{k|t} = \bar{C}^1 \bar{x}_{k|t} + \bar{D}^1 \Delta u_{k|t} \quad (21c)$$

$$\bar{z}_{k|t} = \bar{E}^1 \bar{x}_{k|t} \quad (21d)$$

$$\Delta u_{\min} \leq \Delta u_{k|t} \leq \Delta u_{\max} \quad (21e)$$

$$y_{\min} \leq \bar{y}_{k|t} \leq y_{\max} \quad (21f)$$

$$\bar{x}_{0|t} = \bar{x}(t), u_{-1|t} = \zeta_i u(t-1). \quad (21g)$$

where $\bar{x}_{k|t}$ is the predicted augmented state under the incremental input $\Delta u_{k|t}$ over the horizon T , and $\Delta \mathbf{u} = \text{col}(\Delta u_{0,0|t}, \dots, \Delta u_{N,0|t}, \dots, \Delta u_{N,T-1|t}, \dots, \Delta u_{N,T-1|t})$ is the optimization variable. Note that the prediction model used here is for the nominal configuration $\zeta = \mathbf{1}$ where all units are active $\zeta_i = 1$ for $i = 0, \dots, N$. The reconfigurable model predictive controller integrates the optimal incremental input $\Delta u_{i,k|t}^*$ to obtain the implemented input

$$u_i(t) = \zeta_i u_i(t-1) + \Delta u_{i,0|t}^* \quad (22)$$

for each unit $i = 0, \dots, N$.

The cost function (21a) of the constrained finite-time optimal control problem (21) is configuration-dependent. The term $\zeta_i \bar{z}'_{i,k|t} Q_i \bar{z}_{i,k|t}$ penalizes the performance outputs of the configuration-dependent prediction model (20). For the outdoor unit $i = 0$, the performance output $\bar{z}_0 = z_0 - r_0$ is the difference between the discharge temperature $z_0 = \text{Td}$ and the reference discharge temperature $r_0 = \text{Td}_{\text{ref}}$, which maximizes energy efficiency. Since the outdoor unit is always active $\zeta_0 = 1$, the model predictive control always regulates the discharge temperature. For the indoor units $i = 1, \dots, N$, the performance outputs $\bar{z}_i = \text{col}(z_i - r_i, \xi_i)$ includes the zone temperature tracking errors $z_i - r_i$, and their integrals ξ_i . If an indoor unit is inactive $\zeta_i = 0$, then the zone temperature tracking error and integrated error for that indoor unit do not appear in the cost $\zeta_i \bar{z}'_{i,k|t} Q_i \bar{z}_{i,k|t} = 0$. Thus, the reconfigurable MPC does not regulate the zone temperature of inactive zones.

The term $\lambda_i \Delta u'_{i,k|t} R_i \Delta u_{i,k|t}$ in the cost function (21a) penalizes changes $\Delta u_{i,k|t}$ to the inputs $u_{i,k|t}$. For the outdoor unit $i = 0$, this term penalizes changing the compressor frequency and outdoor fan speed. For the indoor units $i = 1, \dots, N$ this term penalizes changing the capacity command. The scalar λ_i is defined as

$$\lambda_i = \begin{cases} 1 & \text{if } \zeta_i = 1 \\ M & \text{if } \zeta_i = 0 \end{cases} \quad (23)$$

where the “big- M ” scalar M is chosen to be large compared to the eigenvalues of the matrices Q_i , R_i , and P_i . The scalar λ_i ensures the optimal incremental input $\Delta u_{i,k|t}^* = 0$ is zero for inactive indoor units $\zeta_i = 0$ [39]. Thus, the capacity command

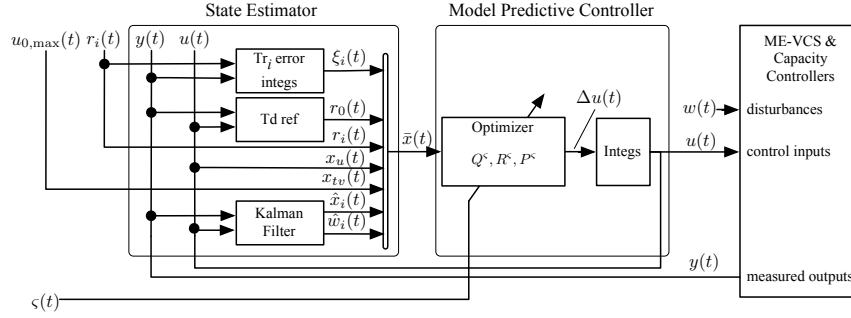


Fig. 9 Block diagram for the reconfigurable MPC. A configuration signal indicating the zones to be turned on modifies the parameterized optimizer.

$u_{i,k|t} = u_{i,k-1|t} + \Delta u_{i,k|t} = 0$ to an inactive room $\zeta_i = 0$ is zero since it is initially zero $u_{i,-1|t} = \zeta_i u_i(t-1)$ and does not change $\Delta u_{i,k|t} = 0$ for $k = 0, \dots, T-1$.

The terminal cost term $\zeta_i \bar{x}_{i,T|t}^T P_i \bar{x}_{i,T|t}$ penalizes the deviation of the augmented state $\bar{x}_{i,N|t}$ for $i = 0, \dots, N$. When the i -th indoor unit is inactive $\zeta_i = 0$, its terminal cost is zero $\zeta_i \bar{x}_{i,T|t}^T P_i \bar{x}_{i,T|t} = 0$. The terminal cost matrices P_i are the Lyapunov matrices for a linear controller designed using the configuration-dependent model (20). The prediction model (21b)–(21d) used by the model predictive controller does not depend on the configuration ζ of the ME-VCS. Instead the optimal control problem (21) uses the model (20) for the nominal configuration $\zeta = \mathbf{1}$. Due to the structure of the cost (21a), solving the optimal control problem (21) with the configuration-independent prediction model (21b)–(21d) is equivalent to solving the problem with the correct configuration-dependent model (20). For more details see [18].

A block diagram summarizing the online calculations performed for the reconfigurable MPC is shown in Fig. 9. The controller is similar to the non-reconfigurable controller (in particular, note that the same estimator is used in Fig. 5), with the exception of a new configuration signal $\zeta(t)$ supplied by external logic. This configuration signal could originate from an occupant indicating that a particular zone is to be turned on ($\zeta_i = 1$), or from a higher level controller that determines whether an indoor unit should become activated based, for example, on the magnitude of the zone error signal e_i . This configuration signal is provided to the optimizer, which is used to modify the cost function (21a) as previously described.

The reconfigurable MPC approach enables zones to be turned on or off, satisfying requirement (E.1). Additionally, because only one set of controller parameters needs to be stored, the memory usage requirements are reduced, which satisfies requirement (E.2). In order to validate the method, experiments are shown wherein external logic automatically deactivates a zone based on the zone temperature error.

5.1.4 Experiment 3: Validation of Reconfigurable MPC

The control system must turn zones on or off automatically in order to regulate zone temperatures when the heat loads are lower than the minimum continuously-available cooling capacity. This requires supervisory logic to compute the system configuration $\zeta(t)$. In this section, a state machine is designed to detect low heat load conditions and reconfigure the ME-VCS automatically, and experiments are presented to validate its performance. The objective of this experiment is to empirically demonstrate reference tracking and constraint enforcement of the reconfigurable MPC controlling a switching system where the dwell times for a particular configuration are determined by a supervisory state machine [40]. The state machine logic considers the sign and magnitude of the zone temperature error signal and associated cooling command to determine when to switch a zone on or off. Specifically, if a zone is off and has become overheated by 1°C , then the state machine will activate that zone. If a zone is active and either the zone has become overcooled by 2.5°C , or the cooling capacity command for that zone has been low enough for long enough, then the zone is deactivated.

Regarding the latter condition, an integrator is used to determine the low actuator condition as follows: If CC_i is less than 40%, then an integrator state $e_i(t)$ increases according to

$$e_i(t+1) = e_i(t) + (40 - CC_i) \quad (24)$$

Once the integrator has reached a predetermined value, then the zone is deactivated. This predetermined value is chosen so that if CC_i has been at its low constraint of 20% for about 5 minutes, then condition (2) becomes true. This test on the capacity command will cause a zone to be deactivated even if good setpoint tracking is achieved, but requires a low capacity command to do so, which is the intended behavior. The parameters used in the state machine have been determined heuristically.

Using this state machine to automatically determine the configuration signal $\zeta(t)$, an experiment is conducted wherein the heat load in zone 2 is reduced. Referring to Fig. 10, the vapor compression system is brought into steady state operation with setpoints $r_1 = 21^\circ\text{C}$, $r_2 = 25^\circ\text{C}$ and the boundary conditions are set to $Q_1 = Q_2 = 1800\text{ W}$, and $\text{OAT} = 35^\circ\text{C}$. At this initial condition, both zone loads are met in steady state with a compressor frequency of $\text{CF} = 40\text{ Hz}$, and capacity commands of $CC_1 = 100\%$ and $CC_2 = 60\%$. At $t = 10\text{ min}$, the heat load in zone 2 is decreased to 500 W (Fig. 10B-iii, red), which is a load that is about equal to the cooling provided when operated at $CC_{2,\min} = 20\%$. As a result of the load step, the temperature in zone 2 is reduced, and the MPC decreases the associated actuator command to its minimum value in an attempt to raise the zone temperature back to the setpoint.

After about 10 min., the integrator in the supervisory state machine has reached its predetermined value, and ζ_2 is set to 0, triggering reconfiguration of the controller. Zone 2 is automatically switched off, and the CC_2 command is set to 0 (Fig. 10A-iii, black), which closes the associated EEV. The zone temperature subsequently increases under the influence of the 500 W load until it becomes overheated

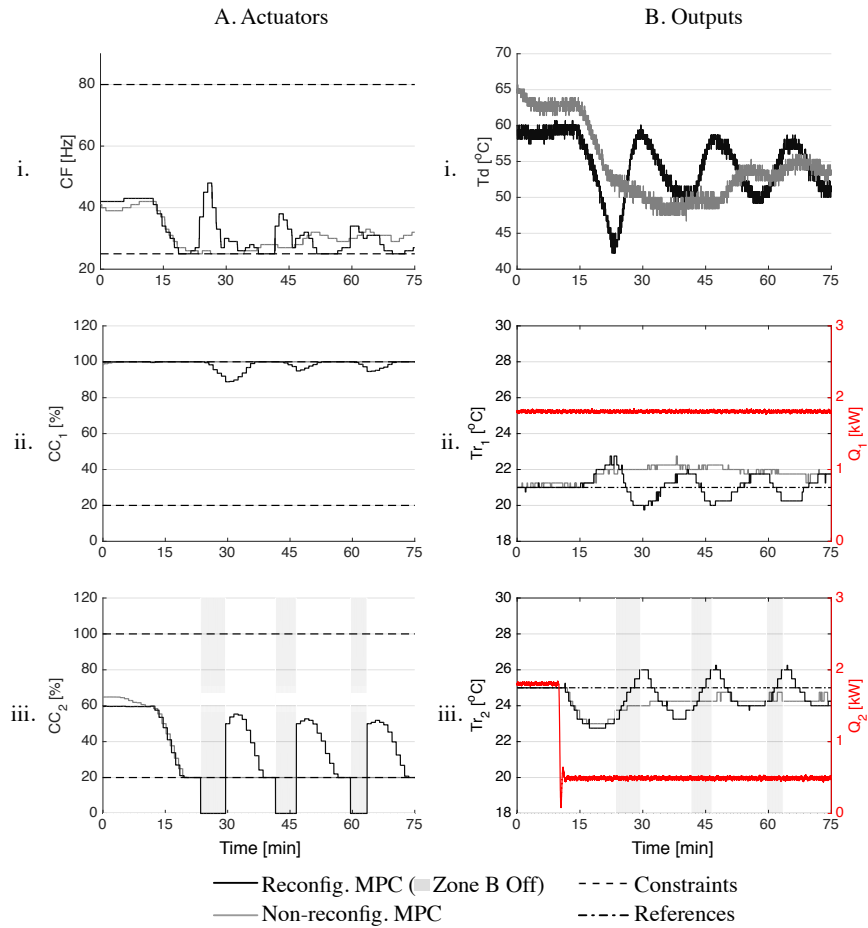


Fig. 10 Reconfig MPC shuts off zones.

by 1°C (Fig. 10B-iii, black), at which point the state machine sets ζ_2 to 1 and the controller is again reconfigured to turn zone 2 back on. This pattern is repeated under automatic control, establishing a cyclic response.

Note that the coupling inherent in the vapor compression system induces a periodic disturbance in zone 1 (Fig. 10B-ii, black) as zone 2 is switched on and off, which can only be partially rejected since the associated actuator CC_1 is saturated at its maximum value for large periods of the disturbance cycle (Fig. 10A-ii, black). Despite the large imbalance in loads between the two zones, both zone temperatures cycle around their respective setpoints, and when averaged over multiple periods, both zones are shown to achieve their setpoints. The experiment demonstrates that the reconfigurable MPC can operate in combination with supervisory logic determining the on/off conditions.

Fig. 10 also shows the same experiment for the case where the controller is not permitted to reconfigure. This non-reconfigurable MPC is shown in gray for the same test conditions. Since the controller cannot turn zone 2 off, CC_2 is driven to its lower limit (Fig. 10A-iii, gray) while CC_1 remains saturated at its upper limit (Fig. 10A-ii, gray). The corresponding temperatures for these zones settle to a nonzero steady state error (about 1°C overheated in zone 1 (Fig. 10B-ii, gray), and about 1°C overcooled in zone 2 (Fig. 10B-iii, gray)). Note that since both zone temperature tracking errors are equally penalized in the cost function, the MPC controller selects compressor frequency commands that equally distribute the zone tracking errors despite both zone capacity commands being saturated.

The experiment presented in this section demonstrates that reconfigurable MPC permits individual zones to be selectively deactivated, satisfying extended requirement (E.1). Further, despite similar transient performance, reconfigurable MPC is much more efficient in memory storage requirements and tuning effort than traditional approaches where an MPC must be created and stored for each configuration and this satisfies extended requirement (E.2).

5.2 Optimization Algorithms for Embedded Platforms

While in general, building control systems may be supported by a fairly powerful computing infrastructure, at the equipment level, the computing platforms are significantly more limited. Thus, in order to solve the finite horizon optimal control problem (14) and (21), HVAC equipment control needs optimization algorithms that are fast, but also simple to allow for implementation in low computational power embedded platforms and for rapid validation.

In general (14) and (21) can be formulated as convex parametric Quadratic Programs (pQPs) with linear equalities and bound constraints

$$\min_{\boldsymbol{\varphi}} \frac{1}{2} \boldsymbol{\varphi}' Q_u \boldsymbol{\varphi} \quad (25a)$$

$$\text{s.t. } G_u \boldsymbol{\varphi} = W_u + S_u \bar{\boldsymbol{x}}(t) \quad (25b)$$

$$\underline{\boldsymbol{\varphi}} \leq \boldsymbol{\varphi} \leq \bar{\boldsymbol{\varphi}} \quad (25c)$$

where $\boldsymbol{\varphi} = \text{col}(\mathbf{x}_t, \Delta \mathbf{u}_t, \mathbf{y}_t)$, $\mathbf{x}_t = \text{col}(\bar{x}_{1|t}, \dots, \bar{x}_{T|t})$, $\mathbf{y}_t = \text{col}(\bar{y}_{0|t}, \dots, \bar{y}_{T-1|t})$, and $\underline{\boldsymbol{\varphi}}$, $\bar{\boldsymbol{\varphi}}$ are constructed from lower and upper bounds on inputs and outputs. Furthermore, the equality constraints in pQP (25) can be eliminated by applying basic concepts in linear systems theory [41] since the real degrees-of-freedom are only the inputs in $\Delta \mathbf{u}$. The result is the pQP

$$\min_{\Delta \mathbf{u}} \frac{1}{2} \Delta \mathbf{u}' Q_p \Delta \mathbf{u} + \mathbf{x}(t)' C_c' \Delta \mathbf{u} \quad (26a)$$

$$\text{s.t. } G_c \Delta \mathbf{u} \leq W_c + S_c \bar{\boldsymbol{x}}(t) \quad (26b)$$

where all the constraints are general linear inequalities.

Over the last few years there has been a large activity in developing simple and fast optimization algorithms for solving (25), (26) as required for MPC [16, 42–49]. In particular the results in Sections 4, 5 are obtained using the PQP method [16] that solves (26) by solving the dual problem

$$\min_{\varphi} \frac{1}{2} \varphi' Q_d \varphi + F_d' \varphi \quad (27a)$$

$$\text{s.t. } \varphi \geq 0, \quad (27b)$$

where $Q_d = G_p Q_p^{-1} G_p'$, $F_d = (G_p Q_p^{-1} C_p + S_p) \bar{x}(t) + W_p$, and then computing $\Delta \mathbf{u}^* = \Gamma_d \theta + \Upsilon_d \varphi^*$, where $\Upsilon_d = -Q_c^{-1} G_c'$, $\Gamma_d = -Q_c^{-1} C_c$. The PQP method solves (27) by iterating

$$[\varphi_{(\ell+1)}]_i = \frac{[(Q_d^- + \phi) \varphi_{(\ell)} + F_d^-]_i}{[(Q_d^+ + \phi) \varphi_{(\ell)} + F_d^+]_i} [\varphi_{(\ell)}]_i \quad (28)$$

where $[a]_i$ is the i^{th} component of vector a , and A^+ , A^- are the positive and negative parts of a matrix A , respectively, until the convergence conditions are reached.

Another algorithm that is most commonly applied to (25) is based on the alternating direction method of multipliers (ADMM), where in order to obtain a simple iteration, a ‘‘copy’’ ζ of the optimization vector φ is used to enforce bound constraints, and the equality between ζ and φ is dualized in the augmented Lagrangian,

$$\min_{\varphi, \zeta} \frac{1}{2} \varphi' Q_u \varphi + \frac{\beta}{2} \|\varphi - \zeta - \lambda\|^2 \quad (29a)$$

$$\text{s.t. } G_p \varphi = K_p \quad (29b)$$

$$\underline{\varphi} \leq \zeta \leq \bar{\varphi} \quad (29c)$$

where λ is the Lagrange multiplier vector and β is a stepsize parameter that can be optimally determined [48, 49]. The ADMM the algorithm iteratively adjusts λ to seek the values of φ , ζ that solve (29) and such that at optimum $\zeta = \varphi$. In [50] the solution is achieved by the iterations

$$\varphi^{(k+1)} = \mathcal{M}(\zeta^{(k)} + \lambda^{(k)}) + \mathcal{N} K_E \quad (30a)$$

$$\zeta^{(k+1)} = \text{proj}_{\zeta \in [\underline{\varphi}, \bar{\varphi}]}(\varphi^{(k+1)} - \lambda^{(k)}) \quad (30b)$$

$$\lambda^{(k+1)} = \lambda^{(k)} + \zeta^{(k+1)} - \varphi^{(k+1)} \quad (30c)$$

where \mathcal{M} , \mathcal{N} are matrices computed from the matrices in (29), and proj denotes the projection, i.e., in this case the clipping within the box determined by $\underline{\varphi}$, $\bar{\varphi}$.

Note that both iterations (28) and (30) involve only basic operations and no additional libraries for algebra operations are required. Hence, both methods are simple to code and to verify and do not impose stringent requirements on the embedded platform, thus enabling the usage of the algorithms in low-cost embedded platforms that are suitable for HVAC equipment. Despite their simplicity, it is shown in [16, 48]

that both methods are relatively fast, and hence allows for solving the finite horizon optimal control problems (14), (21) at rates that are suitable for the target HVAC applications, where the control sampling period is usually on the order of 10–100s.

5.3 Reducing Power Consumption for Demand Response

In the demand response (DR) framework, utilities send signals to consumers to indicate a planned short-term increase in energy rates to incentivize reduced consumption during anticipated periods of expected peak demand. Because HVAC equipment typically consumes significant amounts of energy and users can tolerate a range of temperatures, a small reduction in individual cooling capacity can meaningfully reduce electrical consumption for the utility with minimal impact to zone occupants. Therefore, it is important for HVAC control systems to be responsive to DR requests for reduced consumption.

DR is often realized through zone setbacks. The reduction in energy consumption is an indirect consequence of the setpoint change, and predicting the exact energy reduction depends on equipment details, load conditions and building construction. It is thus difficult to use this approach to reduce energy consumption by a known amount.

However, the model predictive control architecture presented includes a time-varying maximum constraint on the compressor frequency $CF(t) \leq CF_{\max}(t)$, which can be used to directly limit power consumption, provided a performance map (similar to the one represented by Equations (18)-(19) in Chapter 4 **editor: check ref to another chapter**) is available relating compressor speed to power consumption. Suppose a DR event is initiated with the ME-VCS operating in steady state with a non-zero compressor frequency and the heat loads are such that the system does not duty cycle. The supervisory logic receives the DR signal, evaluates the current power consumption, and uses the compressor map to determine the new maximum compressor frequency that results in the desired reduction of energy consumption. This new CF_{\max} is provided to the model predictive controller and the compressor speed is subsequently limited. When a DR event limits compressor speed, the baseline control requirements will continue to be enforced, potentially giving up on setpoint regulation in order to enforce constraints. This strategy has the same effect of allowing zone temperatures to increase as in the zone setback method, but in the case of MPC, the reduction in power consumption is directly specified and reliably achieved.

6 Conclusion

A controller for a commercial vapor compression system must be capable of meeting an extensive set of control objectives. Model predictive control is a design frame-

work that enables satisfaction of both conventional controller requirements (constraint satisfaction, setpoint regulation, etc.), and also requirements not typically discussed in academic treatments of vapor compression system control, including prioritization, design separation-of-concerns and scalability. Through careful architecture considerations, MPC can satisfy requirements for set point regulation, disturbance rejection, energy efficiency, zone on/off, scalability and ease-of-tuning. MPC also enables integration with higher level functionality at the building level. Finally, efficient numerical optimization algorithms have been developed that enable this technology to be deployed into commercial products. We expect this technology to see increased application to this industry in the coming years.

References

1. K. J. Chua, S. K. Chou, and W. M. Yang, "Advances in heat pump systems: A review," *Applied Energy*, vol. 87, no. 12, pp. 3611–3624, December 2010.
2. A. Hepbasli and Y. Kalinci, "A review of heat pump water heating systems," *Renewable and Sustainable Energy Reviews*, vol. 13, no. 6–7, pp. 1211 – 1229, 2009.
3. M. Liu, W. Saman, and F. Bruno, "Development of a novel refrigeration system for refrigerated trucks incorporating phase change material," *Applied Energy*, vol. 92, pp. 336–342, April 2012.
4. S. A. Tassou, G. De-Lille, and Y. T. Ge, "Food transport refrigeration - Approaches to reduce energy consumption and environmental impacts of road transport," *Applied Thermal Engineering*, vol. 29, no. 8-9, pp. 1467–1477, Jun 2009.
5. M. Hawlader, P. K. Dey, S. Diab, and C. Y. Chung, "Solar assisted heat pump desalination system," *Desalination*, vol. 168, no. 0, pp. 49 – 54, 2004.
6. V. Slesarenko, "Heat pumps as a source of heat energy for desalination of seawater," *Desalination*, vol. 139, no. 1–3, pp. 405 – 410, 2001.
7. J. Burger, H. Holland, E. Berenschot, J. Seppenwode, M. ter Brake, H. Gardeniers, and M. Elwenspoek, "169 kelvin cryogenic microcooler employing a condenser, evaporator, flow restriction and counterflow heat exchangers," in *14th IEEE International Conference On Micro Electro Mechanical Systems*, 2001, pp. 418–421.
8. T. Aynur, "Variable refrigerant flow systems: A review," *Energy and Buildings*, vol. 42, pp. 1106–1112, 2010.
9. W. Goetzler, "Variable refrigerant flow systems," *ASHRAE Journal*, vol. 49, no. 4, pp. 24–31, 2007.
10. T. Qureshi and S. Tassou, "Variable-speed capacity control in refrigeration systems," *Applied Thermal Engineering*, vol. 16, no. 2, pp. 103–113, 1996.
11. X.-D. He, S. Liu, and H. H. Asada, "Modeling of vapor compression cycles for multivariable feedback control of HVAC systems," *Journal of Dynamic Systems, Measurement, and Control*, vol. 119, no. 2, pp. 183–191, 1997.
12. X.-D. He, S. Liu, H. H. Asada, and H. Itoh, "Multivariable Control of Vapor Compression Systems," *HVAC&R Research*, vol. 4, no. 3, pp. 205–230, 1998.
13. K. Amano, "Heat pump apparatus and control method thereof," Jun 2012, eP Patent App. EP20,110,007,843. [Online]. Available: <https://www.google.com/patents/EP2469201A2>
14. A. H. Glattfelder and W. Schaufelberger, *Control Systems with Input and Output Constraints*. Springer, 2003.
15. S. Qin and T. Badgwell, "A survey of industrial model predictive control technology," *Control Engineering Practice*, vol. 11, no. 7, pp. 733–764, Jul 2003.

16. S. Di Cairano, M. Brand, and S. A. Bortoff, "Projection-free parallel quadratic programming for linear model predictive control," *International Journal of Control*, vol. 86, no. 8, pp. 1367–1385, 2013.
17. J. M. Maciejowski, *Predictive Control with Constraints*. Pearson Education Limited, 2002.
18. D. J. Burns, C. Danielson, J. Zhou, and S. Di Cairano, "Reconfigurable Model Predictive Control for Multi-Evaporator Vapor Compression Systems," *IEEE Transactions on Control Systems Technology*, under review.
19. J. Bendtsen, K. Trangbaek, and J. Stoustrup, "Plug-and-play control: Modifying control systems online," *IEEE Transactions on Control Systems Technology*, vol. 21, no. 1, pp. 79–93, 2013.
20. J. Stoustrup, "Plug & play control: Control technology towards new challenges," *European Journal of Control*, vol. 15, no. 3, pp. 311–330, 2009.
21. G. Pannocchia and J. B. Rawlings, "Disturbance models for offset-free model-predictive control," *AIChE Journal*, vol. 49, no. 2, pp. 426–437, 2003.
22. U. Maeder, F. Borrelli, and M. Morari, "Linear offset-free model predictive control," *Automatica*, vol. 45, no. 10, pp. 2214–2222, 2009.
23. M. Wallace, B. Das, P. Mhaskar, J. House, and T. Salsbury, "Offset-free model predictive control of a vapor compression cycle," *Journal of Process Control*, vol. 22, no. 7, pp. 1374–1386, 2012.
24. A. Bejan, *Advanced Engineering Thermodynamics*, 3rd ed. Wiley, 2006.
25. P. Li, H. Qiao, Y. Li, J. Seem, J. Winkler, and X. Li, "Recent advances in dynamic modeling of HVAC equipment. Part 1: Equipment modeling," *HVAC&R Research*, vol. 20, no. 1, pp. 136–149, 2014.
26. P. Li, Y. Li, J. Seem, H. Qiao, X. Li, and J. Winkler, "Recent advances in dynamic modeling of HVAC equipment. Part 2: Modelica-based modeling," *HVAC&R Research*, vol. 20, no. 1, pp. 150–161, 2014.
27. M. Ishii and T. Hibiki, *Thermo-Fluid Dynamics of Two-Phase Flow*, 2nd ed. Springer, 2011.
28. C. Laughman, H. Qiao, V. Aute, and R. Radermacher, "A comparison of transient heat pump cycle models using alternative flow descriptions," *Science and Technology for the Built Environment*, vol. 21, no. 5, pp. 666–680, 2015.
29. D. J. Burns and S. A. Bortoff, "Cooling Capacity Control for Multi-Evaporator Vapor Compression Systems," in *16th International Refrigeration and Air Conditioning Conference at Purdue*, 2016.
30. F. Borrelli, A. Bemporad, and M. Morari, *Predictive Control for linear and hybrid systems*, 2015.
31. D. J. Burns, C. R. Laughman, and M. Guay, "Proportional–integral extremum seeking for vapor compression systems," in *Proceedings of the 2016 American Controls Conference*, 2016.
32. D. J. Burns and C. R. Laughman, "Extremum seeking control for energy optimization of vapor compression systems," in *International Refrigeration and Air Conditioning Conference at Purdue*, 2012.
33. S. Di Cairano, H. E. Tseng, D. Bernardini, and A. Bemporad, "Vehicle yaw stability control by coordinated active front steering and differential braking in the tire sideslip angles domain," *Control Systems Technology, IEEE Transactions on*, vol. 21, no. 4, pp. 1236–1248, 2013.
34. D. J. Burns, W. K. Weiss, and M. Guay, "Realtime setpoint optimization with time-varying extremum seeking for vapor compression systems," in *Proceedings of the 2015 American Controls Conference*, 2015.
35. G. Pannocchia and J. B. Rawlings, "Disturbance models for offset-free model-predictive control," *AIChE journal*, vol. 49, no. 2, pp. 426–437, 2003.
36. U. Maeder, F. Borrelli, and M. Morari, "Linear offset-free model predictive control," *Automatica*, vol. 45, no. 10, pp. 2214–2222, 2009.
37. S. Di Cairano, C. A. Pascucci, and A. Bemporad, "The rendezvous dynamics under linear quadratic optimal control," in *Proceedings of the 51st IEEE Conference on Decision and Control*. IEEE, 2012, pp. 6554–6559.
38. S. Di Cairano, "Model adjustable predictive control with stability guarantees," in *American Control Conference (ACC), 2015*, July 2015, pp. 226–231.

39. C. A. Floudas, *Nonlinear and Mixed-Integer Optimization*. Oxford University Press, 1995.
40. L. Bridgeman, C. Danielson, and S. Di Cairano, “Stability and feasibility of mpc for switched linear systems with dwell-time constraints,” in *American Control Conference (ACC)*, 2016.
41. S. Di Cairano and A. Bemporad, “Model predictive control tuning by controller matching,” *Automatic Control, IEEE Transactions on*, vol. 55, no. 1, pp. 185–190, 2010.
42. I. Necoara and J. Suykens, “Application of a smoothing technique to decomposition in convex optimization,” *IEEE Trans. Automatic Control*, vol. 53, no. 11, pp. 2674–2679, 2008.
43. P. Giselsson, “Execution time certification for gradient-based optimization in model predictive control,” in *Proc. 51st IEEE Conference on Decision and Control*, Maui, HI, 2012, pp. 3165–3170.
44. M. Kögel and R. Findeisen, “Fast predictive control of linear systems combining Nesterov’s gradient method and the method of multipliers,” in *Proc. 50th IEEE Conference on Decision and Control*, Orlando, FL, 2011, pp. 501–506.
45. S. Richter, C. N. Jones, and M. Morari, “Computational complexity certification for real-time mpc with input constraints based on the fast gradient method,” *IEEE Trans. Automatic Control*, vol. 57, no. 6, pp. 1391–1403, 2012.
46. P. Patrinos and A. Bemporad, “An accelerated dual gradient-projection algorithm for embedded linear model predictive control,” *IEEE Trans. Automatic Control*, vol. 59, no. 1, pp. 18–33, 2014.
47. E. Ghadimi, A. Teixeira, I. Shames, and M. Johansson, “Optimal parameter selection for the alternating direction method of multipliers (admm): quadratic problems,” *IEEE Trans. Automatic Control*, vol. 60, no. 3, pp. 644–658, 2015.
48. A. U. Raghunathan and S. Di Cairano, “Optimal step-size selection in alternating direction method of multipliers for convex quadratic programs and model predictive control,” in *Proc. Symp. Mathematical Theory of Networks and Systems*, 2014, pp. 807–814.
49. A. U. Raghunathan and S. Di Cairano, “Infeasibility detection in alternating direction method of multipliers for convex quadratic programs,” in *Proc. 53rd IEEE Conference on Decision and Control*, 2014, pp. 5819–5824.
50. A. U. Raghunathan and S. Di Cairano, “ADMM for convex quadratic programs: Q-linear convergence and infeasibility detection,” *arXiv preprint arXiv:1411.7288*, 2014.